

# Methylammonium-Mediated Evolution of Mixed-Organic-Cation Perovskite Thin Films: A Dynamic Composition-Tuning Process

Chongwen Li<sup>+</sup>, Yuanyuan Zhou<sup>+</sup>, Li Wang, Yue Chang, Yingxia Zong, Lioz Etgar, Guanglei Cui,\* Nitin P. Padture, and Shuping Pang\*

**Abstract:** Methylammonium-mediated phase-evolution behavior of  $FA_{1-x}MA_xPbI_3$  mixed-organic-cation perovskite (MOCP) is studied. It is found that by simply enriching the MOCP precursor solutions with excess methylammonium cations, the MOCPs form via a dynamic composition-tuning process that is key to obtaining MOCP thin films with superior properties. This simple chemical approach addresses several key challenges, such as control over phase purity, uniformity, grain size, composition, etc., associated with the solution-growth of MOCP thin films with targeted compositions.

Since the first use of hybrid organic–inorganic perovskites (HOIPs) in solar cells in 2009,<sup>[1]</sup> the power conversion efficiency (PCE) of perovskite-based solar cells (PSCs) has shot up to over 22% within a short period of time.<sup>[2]</sup> Methylammonium lead iodide ( $CH_3NH_3PbI_3$  or  $MAPbI_3$ ) has been the most widely studied HOIP for PSCs in the past.<sup>[3–9]</sup> However, there are several issues with  $MAPbI_3$ , including the less-than-ideal band gap<sup>[7,8]</sup> and low intrinsic thermal stability,<sup>[10]</sup> thus calling for the development of HOIPs of other compositions. Formamidinium lead triiodide ( $HC(NH_2)_2PbI_3$  or  $FAPbI_3$ ) HOIP has become a promising alternative that exhibits a relatively smaller band gap and much better thermal stability.<sup>[11–13]</sup> However,  $FAPbI_3$  has two polymorphs at room temperature—the “black” perovskite  $\alpha$ -phase and the “yellow” non-perovskite  $\delta$ -phase. But the desirable  $\alpha$ -phase appears to be unstable in ambient atmosphere.<sup>[12–17]</sup> In this context,  $FA_{1-x}MA_xPbI_3$  mixed-organic-cation perovskites (MOCPs) with relatively larger content of  $FA^+$  cations (typically  $FA_{0.8}MA_{0.2}PbI_3$ ) are becoming state-of-

the-art compositions. This is because MOCPs show combined merits of enhanced light-absorption and better thermal/environmental stability. In fact, MOCPs and/or their variants have been used to demonstrate the best-performing PSCs.<sup>[17–21]</sup> Despite their attractive properties, research on MOCPs and MOCPs-based PSCs has been held back because of the difficulty in the synthesis of MOCPs, which is mainly due to the following reasons. First, the formation of the undesirable  $\delta$ -phase non-perovskite byproduct that typically accompanies MOCPs synthesis will compromise the phase purity of the obtained MOCPs. Second, a higher annealing temperature ( $>150^\circ\text{C}$ ), compared with that needed for  $MAPbI_3$ , is usually required for crystallizing MOCPs from solution.<sup>[17–21]</sup> This results in a moderate nucleation rate and high growth rate, which is not desirable for the formation of uniform thin films from solutions.<sup>[4]</sup> Thus, control over the uniformity and microstructures (e.g. grain size) of the solution-grown MOCPs thin films is challenging. Third, it is a challenge to obtain MOCPs thin films with the exact targeted compositions. For example, the popular “two-step” methods<sup>[5,9]</sup> that have been highly successful in depositing single-organic-cation HOIP ( $MAPbI_3$  or  $FAPbI_3$ ) thin films are being considered for MOCPs.<sup>[21]</sup> However, in order to achieve a targeted MOCP composition, one needs precise control over the competing diffusion kinetics of  $MA^+$  and  $FA^+$  into the pre-deposited  $PbI_2$  solid films, which is, in fact, very difficult.<sup>[4]</sup>

Here we report a methylammonium-mediation (MAM) approach that addresses all the aforementioned issues in the solution synthesis of MOCP thin films. This approach involves simple addition of excess  $MA^+$  cations into a stoichiometric MOCP precursor solution, which tailors the chemistry of MOCP evolution from the solution. This results in the ready formation of phase-pure, uniform, large-grain, and exact-composition MOCP thin films. PSCs fabricated using MAM-processed MOCP thin films are shown to deliver PCEs as high as 19%.

The MAM approach may appear similar to the simple additive-assisted synthetic protocols that are widely used for the solution-deposition of single-cation HOIPs.<sup>[4,7,22,23]</sup> However, the underlying reaction chemistry in the MAM approach is actually unique, as illustrated schematically in Figure 1. The ions shown (Figure 1) in the precursor solution are generally random and disordered. In this study, these ions are formed in the solution by dissolving  $FAI$ ,  $MAI$ ,  $PbI_2$  and  $MAX$  precursors in specific ratios (e.g.  $0.8MAI\cdot 0.2FAI\cdot PbI_2\cdot MAX$  for obtaining  $FA_{0.8}MA_{0.2}PbI_3$  MOCP), where spontaneous ion-exchange in the solution allows the redistribution/movement of the ions in an equilibrium state.<sup>[24]</sup>

[\*] C. Li,<sup>[†]</sup> Y. Chang, Y. Zong, Dr. G. Cui, Dr. S. Pang  
Qingdao Institute of Bioenergy and Bioprocess Technology  
Chinese Academy of Sciences  
Qingdao, 266101 (P.R. China)  
E-mail: cuiigl@qibebt.ac.cn  
pangsp@qibebt.ac.cn

Dr. Y. Zhou,<sup>[†]</sup> Y. Zong, Prof. N. P. Padture  
School of Engineering, Brown University  
Providence, RI 02912 (USA)

Dr. L. Wang, Y. Zong  
Qingdao University of Science and Technology  
Qingdao, 266042 (P.R. China)

Dr. L. Etgar  
Institute of Chemistry, The Hebrew University of Jerusalem  
Jerusalem 91904 (Israel)

[†] These authors contributed equally to this work.

Supporting information and the ORCID identification number(s) for the author(s) of this article can be found under:  
<https://doi.org/10.1002/anie.201704188>.

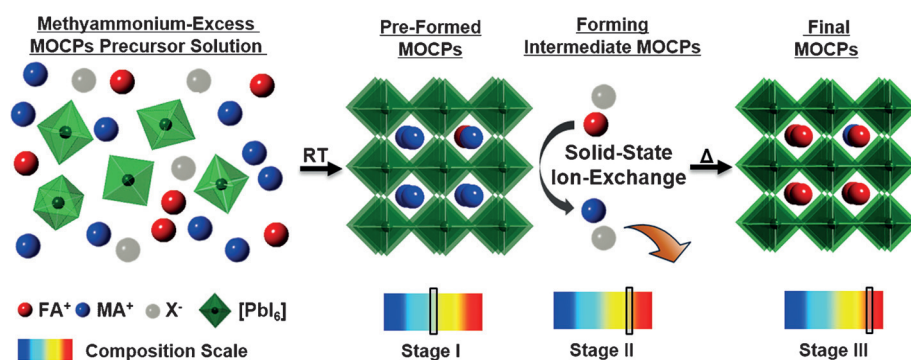


**Figure 1.** MAM synthesis of  $\text{FA}_{1-x}\text{MA}_x\text{PbI}_3$  MOCP from  $\text{MA}^+$ -excess precursor solutions.  $\text{X}^-$  represents an anion that does not fit into the MOCP structure. While  $\text{X}^- = \text{Cl}^-$  is a rational choice with suitable volatility during the MAM synthesis, there may be other choices besides  $\text{Cl}^-$ . The composition scale bar indicates schematically the approximate composition of the MOCP phase at each stage, with left (blue) and right (red) extremes representing pure  $\text{MAPbI}_3$  and  $\text{FAPbI}_3$ , respectively.

Note that the addition of excess  $\text{MA}^+$  cations must be coupled with  $\text{X}^-$  anions to maintain neutral charge in the solution. In order not to affect the composition of the final MOCPs,  $\text{X}^-$  must be an anion that does not fit in the MOCP crystalline structure, and it exhibits suitable volatility for solution processing. Based on these considerations,  $\text{MACl}$  is selected to be the source of excess  $\text{MA}^+$ .<sup>[25]</sup> Once the  $\text{MA}^+$ -excess MOCP solution is spin-coated, supersaturation of the solution occurs due to the centrifugal force, which induces the nucleation and growth of MOCP thin films at room temperature (RT). The pre-formed MOCP at this stage (Stage I) is expected to contain a relatively larger fraction of  $\text{MA}^+$  cations as its crystallization occurs from the  $\text{MA}^+$ -rich environment. During the subsequent thermal-annealing step, since  $\text{FA}^+$ -rich HOIPs are thermodynamically more stable phases at elevated temperatures, an ion-exchange reaction occurs between Stage-I MOCP and the surrounding  $\text{FA}^+$  cations,<sup>[25,26]</sup> leading to the gradual enrichment of  $\text{FA}^+$  in the MOCPs. This continues until the  $\text{FA}^+$  cations outside the MOCP phases are fully depleted, at which stage (Stage III) the final MOCP forms. For describing the MAM process more clearly, Stage II is introduced, which corresponds to the thin film state when the thermally induced ion-exchange process is interrupted. The composition of Stage-II MOCP has an  $\text{FA}^+/\text{MA}^+$  ratio in-between that of Stage-I and Stage-III MOCP. Overall, during the MAM process, the composition of the as-formed MOCP is dynamically tuned with the  $\text{FA}^+/\text{MA}^+$  ratio increasing in the thin film, and this process results in the desired MOCP of the exact prescribed composition. This unique process avoids the formation of the undesirable “yellow”  $\delta$ -phase because the initially formed  $\text{MA}^+$ -rich HOIP does not energetically favor its existence as a non-perovskite  $\delta$ -phase.

To confirm the proposed mechanisms in Figure 1, the phase evolution in the MAM process is investigated further. Here, we have focused on a starting precursor composition of  $\text{FA}_{0.8}\text{MA}_{0.2}\text{PbI}_3\text{-MACl}$  as a case study. Figure 2 shows XRD patterns and UV-vis spectra of the Stage-I, Stage-II, and Stage-III thin films. In the XRD results in Figure 2A, well-resolved characteristic peaks are observed, which confirms the crystalline MOCP phases at all stages. A closer look at the

MOCP characteristic peak shows a gradual shift to lower  $2\theta$  going from Stage I to Stage III, indicating expansion of the MOCP crystal lattice. The lattice parameters of the quasi-cubic perovskite crystal unit are calculated to be 6.300 Å, 6.310 Å, and 6.335 Å for the Stage-I, Stage-II, and Stage-III thin films, respectively. Figure 2B shows absorption-edge red-shift from 800 nm to 815 nm going from Stage I to Stage III. Using the Tauc plots in Figure S1 (in the Supporting Information (SI)), the band gaps of the Stage-I, Stage-II, and Stage-III thin films are determined to be 1.560 eV, 1.550 eV, and

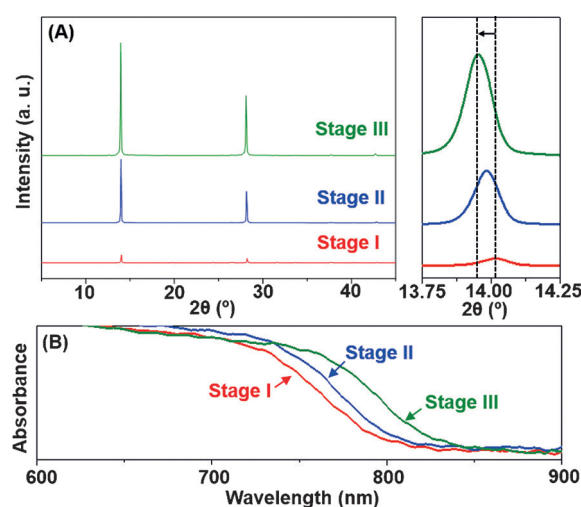


**Figure 2.** A) XRD patterns and B) UV-vis spectra of the Stage-I, Stage-II and Stage-III thin films, which are fabricated by annealing the film at 25 °C, 100 °C, and 150 °C for 30 min, respectively.  $\text{FAI}:\text{MAI}:\text{PbI}_2:\text{MACl}$  ratio is 0.8:0.2:1:1.

1.535 eV, respectively. Both the XRD and the UV-vis results confirm the dynamic composition-tuning process, which are consistent with the proposed solid-state ion-exchange mechanisms hypothesized in Figure 1.

In order to ascertain the exact composition of the thin films at each stage, XRD patterns and UV-vis spectra are recorded for a series of  $\text{FA}_{1-x}\text{MA}_x\text{PbI}_3$  MOCP thin films, with  $x = 0.1, 0.2, 0.3, 0.4, 0.5, 0.6, 0.7, 0.8, 0.9,$  and 1.0, and are presented in Figure S2 in the SI. The lattice parameter of each MOCP phase is calculated, and the band gap is determined by data-fitting; the results are shown in Figure 3. A linear equation ( $a = 6.3516 - 0.0845x$ ) and a polynomial equation ( $E_g = 1.5352 + 0.0133x + 0.0530x^2$ ) can be used to describe empirically the lattice parameter ( $a$ ) and the band gap ( $E_g$ ) of thin films, respectively, as a function of  $x$ . This is very similar to what was reported in the case of  $\text{MAPbI}_{1-x}\text{Br}_x$ .<sup>[27]</sup> By using these two equations, the Stage-I, Stage-II, and Stage-III thin

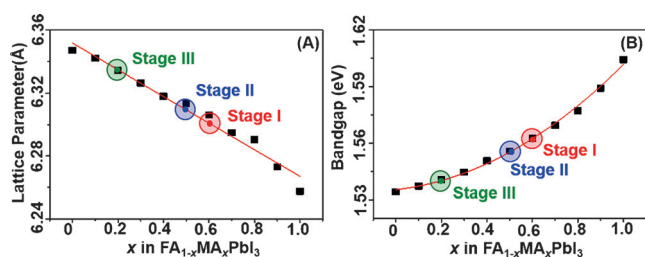
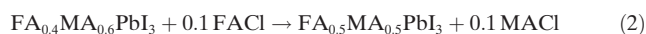


**Figure 3.** A) XRD patterns and B) UV-vis spectra of Stage-I, Stage-II, and Stage-III thin films.

film compositions are determined as FA<sub>0.4</sub>MA<sub>0.6</sub>PbI<sub>3</sub>, FA<sub>0.5</sub>MA<sub>0.5</sub>PbI<sub>3</sub>, and FA<sub>0.8</sub>MA<sub>0.2</sub>PbI<sub>3</sub>, respectively (labeled in Figure 3). This clarifies the exact chemical reactions, along with the MAM evolution of FA<sub>0.8</sub>MA<sub>0.2</sub>PbI<sub>3</sub> MOCP, which are as follows [Eqs. (1)–(4)]:



At Stage I, Reaction 1 occurs at RT, and FA<sub>0.4</sub>MA<sub>0.6</sub>PbI<sub>3</sub> forms as well as the FAX by-product. After heating to some extent, Stage II is reached, which depletes some of the as-formed FAX by-product and FA<sub>0.5</sub>MA<sub>0.5</sub>PbI<sub>3</sub> forms (Reaction 2). Further heating induces Reaction 3, which involves the ion-exchange reaction between the FAX residue with FA<sub>0.5</sub>MA<sub>0.5</sub>PbI<sub>3</sub>, FA<sub>0.8</sub>MA<sub>0.2</sub>PbI<sub>3</sub> forms at this stage (Stage III). During annealing, MAX decomposes/sublimes (Reaction 4),<sup>[22,23]</sup> which drives the progression of Reactions 2 and 3. The molar ratio of FA<sup>+</sup>:MA<sup>+</sup> in Stage-II thin film is determined to be 1:0.62 using nuclear magnetic resonance (NMR) spectroscopy (see Figure S3 in the SI), which implies that Stage-II thin film consists of FA<sub>0.5</sub>MA<sub>0.5</sub>PbI<sub>3</sub> MOCP and excess 0.3 FACl. This is consistent with the fact that the MACl by-products from solid-state ion-exchange reactions are released instantaneously via Reaction 4. In this context, the proposed reactions are fully consistent with our experimental results.

Isothermal annealing experiments were also conducted, where the as-spinc coated film was annealed at two different

constant temperatures of 100 °C and 150 °C, and the absorption spectra of the film with different isothermal annealing time were recorded in Figure S4 in the SI. The absorption edge of the film gradually red-shifts until 815 nm, which reflects the composition-tuning process. At a higher annealing temperature, the composition-tuning kinetics are more rapid, which is consistent with the proposed MOCP crystallization mechanism in Figure 1.

To explore the generality of the MAM evolution behavior of MOCPs, experiments similar to those in Figure 2 were performed with a starting precursor composition of 0.6MAI·0.4FAI·PbI<sub>2</sub>·MAX (X = Cl). The results shown in Figure S5 in the SI indicate that the MAM evolution also occurs in this case. Additional NMR experiments (Figure S6 in the SI) on the MAM-processed MOCP samples were performed, which confirm that the as-obtained thin films have the exact targeted MOCP compositions. The effect of X<sup>-</sup> on the MAM evolution behavior of MOCPs is further studied. When X<sup>-</sup> is an anion, such as CH<sub>3</sub>COO<sup>-</sup> (Ac<sup>-</sup>) with higher volatility than Cl<sup>-</sup>, the dominant hybrid mixed-organic-cation compound formed from the same process is non-perovskite, as shown in Figure S7 in the SI. This is because of the release of MAAc during the RT spin-coating process, which results in insufficient MA<sup>+</sup> content in the as-precipitated phases, which leads to the formation of FA-based non-perovskite compounds. The NMR result in Figure S8 in the SI confirms the substantial release of MAAc during spin-coating. When X<sup>-</sup> is I<sup>-</sup>, which is less volatile than Cl<sup>-</sup>, the MAM evolution behavior of MOCPs still occurs (see Figure S9 in the SI), but it requires much longer annealing time. These results highlight the significance of the volatility of X<sup>-</sup> anions in the successful MAM synthesis of MOCP thin films.

The microstructural evolution of MOCPs during the MAM process is further investigated. Figure 4 shows SEM images of the top surfaces of Stage-I, Stage-II, and Stage-III thin films. In Figure 4A (Stage I), a continuous microstructure with full coverage is observed in the thin film. However, the grain structure is not well-defined, which is clearly related to the presence of multiple and mixed phases. The estimated grain size of the crystalline phases of FA<sub>0.4</sub>MA<sub>0.6</sub>PbI<sub>3</sub> MOCP in the thin film is only ca. 200 nm, which is to be expected considering that the processing is performed at RT.<sup>[4]</sup> The FAX and/or MAX phases are not distinguishable in the SEM considering due to their low crystallinity, as indicated by the XRD results (Figure 2A). With the progression of Reactions 2 and 3, the MOCP grains gradually become larger,

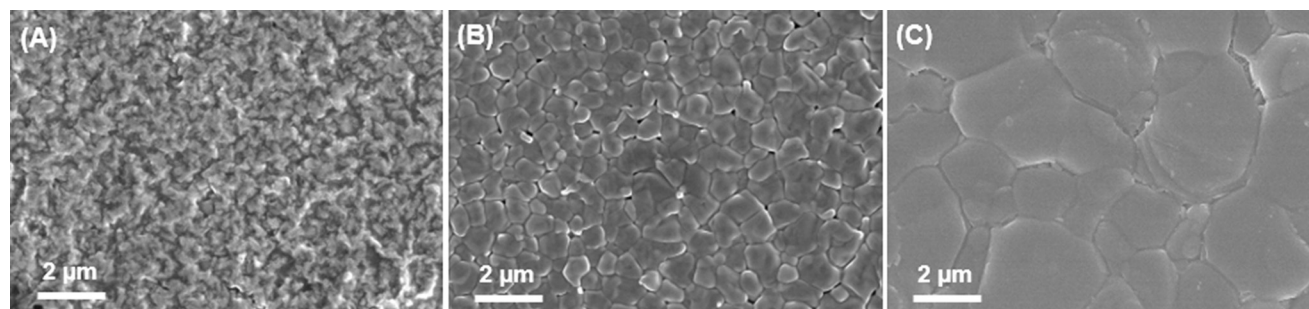


**Figure 4.** Top-view SEM images of the surface of: A) Stage-I, B) Stage-II, and C) Stage-III thin films. FAI:MAI:PbI<sub>2</sub>:MACl ratio is 0.8:0.2:1:1.

which is expected considering the starting fine-grain microstructure and the inevitable coarsening at elevated temperatures. The final  $\text{FA}_{0.8}\text{MA}_{0.2}\text{PbI}_3$  MOCP thin film (Stage III) shows a mean grain size of ca. 2  $\mu\text{m}$ , with occasional grains as large as 4  $\mu\text{m}$  (Figure S10 in the SI), as determined using image analyses based on 78 grains.<sup>[29]</sup> This is more than six times the thickness of the film (ca. 500 nm). This is striking, as generally the grain size in thermally-coarsened polycrystalline thin films is limited by the film thickness.<sup>[4]</sup> In this context, we have investigated the effect of MA<sup>+</sup> amount on the microstructure of the final MOCP thin films. The results in Figure S11 in the SI suggest that, in addition to thermal energy, the MA<sup>+</sup>-cations appear to play a significant role in the grain coarsening, as well as the MOCP thin film coverage. This is reminiscent of numerous studies in the literature on the role of additives in the crystallization of HOIPs.<sup>[4,7,22,23]</sup> It is interesting to note that accompanying the grain coarsening, there is a silent composition-tuning process occurring, as discussed above. Such composition-tuning coupled microstructural evolution mechanisms are not well understood, which await further elucidation in the future. Nevertheless, to the best of our knowledge,<sup>[17–21]</sup> the phase-pure, full-coverage  $\text{FA}_{0.8}\text{MA}_{0.2}\text{PbI}_3$  MOCP thin film with ca. 2  $\mu\text{m}$  mean grain size obtained here is unprecedented. Furthermore, the composition in the final MOCP thin film is uniform over the entire substrate, as confirmed from the photoluminescence (PL) spectra measured at several different locations on the film (see Figure S12 in the SI).

The  $\text{FA}_{0.8}\text{MA}_{0.2}\text{PbI}_3$  MOCP thin films grown using the MAM process were assembled into PSCs for assessing their photovoltaic (PV) performance; Figure 5A shows a cross-sectional view of one such PSC. The PSC structure consists of

the MOCP layer sandwiched between a FTO/mesostructured  $\text{TiO}_2$  electron-extracting anode and a Spiro-OMeTAD/Au hole-extracting cathode. The ca. 200 nm thick mesoporous  $\text{TiO}_2$  layer is fully infiltrated by the MOCP, and a 500 nm thick MOCP capping layer forms on the top of the  $\text{TiO}_2$  layer. The MOCP grains appear very large and dense, with only vertical grain boundaries visible, confirming the desirable microstructure of MAM-processed MOCPs in the PSC.<sup>[29]</sup> Figure 5B shows the current density ( $J$ )–voltage ( $V$ ) curves of the PSC under reverse and forward scans, showing a PCE of 18.7% and 18.4%, respectively. Negligible  $J$ – $V$  hysteresis is observed, indicating balanced charge transport in the PSC.<sup>[30]</sup> This is probably due to the combined merits of the large grains, the presence of only vertical grain boundaries, the desirable MOCP composition, and the use of mesostructured  $\text{TiO}_2$ . It appears that this unique microstructure and composition of the MOCP grains may also be responsible for the negligible hysteresis because  $J$ – $V$  hysteresis has been frequently observed in our previously reported PSCs with similar device architecture, but with fine-grained single-organic-cation HOIP thin films.<sup>[31]</sup> External quantum efficiency (EQE) was also measured, showing an integrated current density of 21.40  $\text{mA cm}^{-2}$  (Figure 5C), which is close to the short circuit current density ( $J_{\text{sc}}$ ) reported in Figure 5B. The stabilized current/power output is monitored at the maximum power point of 0.85 V; a very similar PCE of 18.2% (compared to the  $J$ – $V$  results) is observed in Figure 5D. The high reproducibility afforded by the MAM method in fabricating high-performance PSCs is also demonstrated in Figure S13 in the SI. The stability of a typical MAM-processed MOCP-based PSC was also evaluated and the results are reported in Figure S14 in the SI. The PSC shows ca.

80% retention of its initial PCE after 500-h exposure to the ambient (ca. 20% relative humidity, RT). This outstanding PV performance affirms the efficacy of the MAM method for the reliable fabrication of high-quality MOCP thin films.

In closing, we report here an effective approach that uses excess MA<sup>+</sup> in the precursor solution to mediate the solution growth of  $\text{FA}_{1-x}\text{MA}_x\text{PbI}_3$  MOCP thin films. The investigations into the phase and microstructural evolution of the MOCP thin films provide insights into this MAM process. It is discovered that the evolution of the coarse-grained MOCP microstructures is coupled with unprecedented dynamic composition-tuning, which is key to the success of the MAM approach. This study represents a new research direction in exploring unprecedented phenomena related to the highly complex HOIP material systems in a vast composition space.

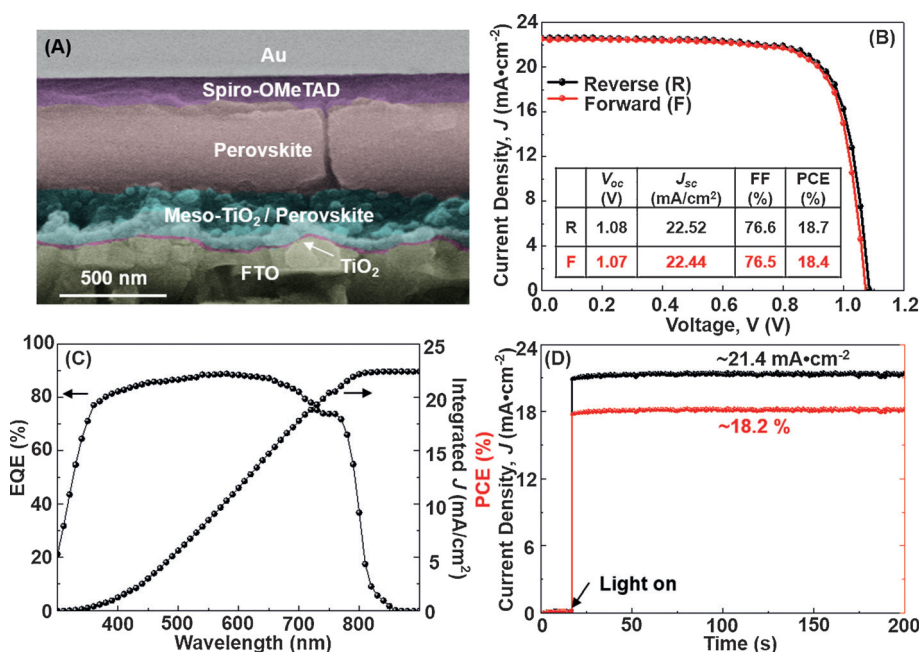


**Figure 5.** A) Cross-sectional SEM image (false color) of a  $\text{FA}_{0.8}\text{MA}_{0.2}\text{PbI}_3$ -MOCP-based PSCs made using the MAM method. B)  $J$ – $V$  curves of the PSC under one-sun illumination under reverse and forward scans. Inset: PV parameters. C) EQE and integrated  $J$  plots from the same PSC. D) Stabilized PCE and  $J$  at maximum power point of the same PSC.

## Acknowledgements

Financial support from the International S&T Cooperation Program of China (2015DFG62670), National Natural Science Foundation of China (51672290, 21671196, 61604156), Basic Research Program of Qingdao (15-9-1-17-jch, KJZD-14-38-JCH), the Youth Innovation Promotion Association of CAS (2015167) and the Qingdao Key Lab of Solar Energy Utilization and Energy Storage Technology, and the U.S. National Science Foundation (DMR-1305913 and OIA-1538893) is gratefully acknowledged.

## Conflict of interest

The authors declare no conflict of interest.

**Keywords:** crystal growth · hybrid perovskites · solar cells · thin films

**How to cite:** *Angew. Chem. Int. Ed.* **2017**, *56*, 7674–7678  
*Angew. Chem.* **2017**, *129*, 7782–7786

- [1] A. Kojima, K. Teshima, Y. Shirai, T. Miyasaka, *J. Am. Chem. Soc.* **2009**, *131*, 6050–6051.
- [2] [http://www.nrel.gov/pv/assets/images/efficiency\\_chart.jpg](http://www.nrel.gov/pv/assets/images/efficiency_chart.jpg), Accessed on 20 December **2016**.
- [3] D. B. Mitzi, In *Progress in Inorganic Chemistry Vol. 48* (Ed.: K. D. Karlin), Wiley, New York, **1999**, pp. 1–122.
- [4] Y. Zhou, O. S. Game, S. Pang, N. P. Padture, *J. Phys. Chem. Lett.* **2015**, *6*, 4827–4839.
- [5] J. Burschka, N. Pellet, S. J. Moon, R. Humphry-Baker, P. Gao, M. K. Nazeeruddin, M. Grätzel, *Nature* **2013**, *499*, 316–319.
- [6] Y. Zhou, M. Yang, W. Wu, A. L. Vasiliev, K. Zhu, N. P. Padture, *J. Mater. Chem. A* **2015**, *3*, 8178–8184.
- [7] Y. Zhao, K. Zhu, *Chem. Soc. Rev.* **2016**, *45*, 655–689.
- [8] W. Zhang, G. E. Eperon, H. J. Snaith, *Nat. Energy* **2016**, *1*, 16048.
- [9] Z. Xiao, C. Bi, Y. Shao, Q. Dong, Q. Wang, Y. Yuan, C. Wang, Y. Gao, J. Huang, *Energy Environ. Sci.* **2014**, *7*, 2619–2623.
- [10] G. P. Nagabhushana, R. Shivaramaiah, A. Navrotsky, *Proc. Natl. Acad. Sci. USA* **2016**, *113*, 7717–7721.
- [11] G. E. Eperon, S. D. Stranks, C. Menelaou, M. B. Johnston, L. M. Herz, H. J. Snaith, *Energy Environ. Sci.* **2014**, *7*, 982–988.
- [12] C. C. Stoumpos, C. D. Malliakas, M. G. Kanatzidis, *Inorg. Chem.* **2013**, *52*, 9019–9038.
- [13] S. Pang, H. Hu, J. Zhang, S. Lv, Y. Yu, F. Wei, T. Qin, H. Xu, Z. Liu, G. Cui, *Chem. Mater.* **2014**, *26*, 1485–1491.
- [14] Z. Wang, Y. Zhou, S. Pang, Z. Xiao, J. Zhang, W. Chai, H. Xu, Z. Liu, N. P. Padture, G. Cui, *Chem. Mater.* **2015**, *27*, 7149–7155.
- [15] Y. Zhou, M. Yang, S. Pang, K. Zhu, N. P. Padture, *J. Am. Chem. Soc.* **2016**, *138*, 5535–5538.
- [16] Z. Li, M. Yang, J.-S. Park, S.-H. Wei, J. J. Berry, K. Zhu, *Chem. Mater.* **2016**, *28*, 284–292.
- [17] N. Pellet, P. Gao, G. Gregori, T. Y. Yang, M. K. Nazeeruddin, J. Maier, M. Grätzel, *Angew. Chem. Int. Ed.* **2014**, *53*, 3151–3157; *Angew. Chem.* **2014**, *126*, 3215–3221.
- [18] X. Li, D. Bi, C. Yi, J.-D. Décoppet, J. Luo, S. M. Zakeeruddin, A. Hagfeldt, M. Grätzel, *Science* **2016**, *353*, 58–62.
- [19] M. Saliba, T. Matsui, J.-Y. Seo, K. Domanski, J.-P. Correa-Baena, M. K. Nazeeruddin, S. M. Zakeeruddin, W. Tress, A. Abate, A. Hagfeldt, M. Grätzel, *Energy Environ. Sci.* **2016**, *9*, 1989–1997.
- [20] D. Bi, W. Tress, M. I. Dar, P. Gao, J. Luo, C. Renevier, K. Schenk, A. Abate, F. Giordano, J.-P. C. Baena, J.-D. Decoppet, S. M. Zakeeruddin, M. K. Nazeeruddin, M. Grätzel, A. Hagfeldt, *Sci. Adv.* **2016**, *2*, e1501170.
- [21] J. Liu, Y. Shirai, X. Yang, Y. Yue, W. Chen, Y. Wu, A. Islam, L. Han, *Adv. Mater.* **2015**, *27*, 4918–4923.
- [22] H. Yu, F. Wang, F. Xie, W. Li, J. Chen, N. Zhao, *Adv. Funct. Mater.* **2014**, *24*, 7102–7108.
- [23] Y. Zhao, K. Zhu, *J. Phys. Chem. C* **2014**, *118*, 9412–9418.
- [24] C. Li, Z. Wang, Y. Chang, Y. Zong, F. Ji, B. Zhang, H. Li, S. Pang, *RSC Adv.* **2016**, *6*, 85026–85029.
- [25] G. E. Eperon, C. E. Beck, H. J. Snaith, *Mater. Horiz.* **2016**, *3*, 63–71.
- [26] F. Ji, L. Wang, S. Pang, P. Gao, H. Xu, G. Xie, J. Zhang, G. Cui, *J. Mater. Chem. A* **2016**, *4*, 14437–14443.
- [27] J. H. Noh, S. H. Im, J. H. Heo, T. N. Mandal, S. I. Seok, *Nano Lett.* **2013**, *13*, 1764–1769.
- [28] N. Wang, Y. Zhou, M.-G. Ju, H. F. Garces, T. Ding, S. Pang, X. C. Zeng, N. P. Padture, X. W. Sun, *Adv. Energy Mater.* **2016**, *6*, 16001130.
- [29] J. Huang, Y. Shao, Q. Dong, *J. Phys. Chem. Lett.* **2015**, *6*, 3218–3227.
- [30] K. Chen, Q. Hu, T. Liu, L. Zhao, D. Luo, J. Wu, Y. Zhang, W. Zhang, F. Liu, T. P. Russell, R. Zhu, Q. Gong, *Adv. Mater.* **2016**, *28*, 10718–10724.
- [31] S. Pang, Y. Zhou, Z. Wang, M. Yang, A. R. Krause, Z. Zhou, K. Zhu, N. P. Padture, G. Cui, *J. Am. Chem. Soc.* **2016**, *138*, 750–753.

Manuscript received: April 23, 2017

Version of record online: May 19, 2017